# Microstructure and mechanical properties of lead-free solders and solder joints used in microelectronic applications

S. K. Kang P. A. Lauro D.-Y. Shih D. W. Henderson K. J. Puttlitz

The replacement of lead (Pb)-bearing solders used in the electronic industry with Pb-free solders will become a reality in the near future. Several promising Pb-free solders have recently been identified, including Sn-0.7Cu, Sn-3.5Ag, Sn-3.8Ag-0.7Cu, and Sn-3.5Ag-4.8Bi (in wt.% with slight variations in composition). These are all Sn-rich solders with melting temperatures between 210°C and 227°C, and are recommended for various soldering applications, including surface mount technology (SMT), plated-through-hole (PTH), ball grid array (BGA), flip-chip bumping, and others. Although a considerable amount of information on Pb-free solders has been published in the last few years, the database on these new materials is still at an infant stage compared with that for Pb-containing solders. This paper addresses several aspects of the current fundamental materials understanding associated with Pb-free solders and various issues regarding their imminent use in electronic interconnect applications, including microstructure-processingproperty relations, mechanical properties, interfacial reactions, and the thermal-fatigue life and failure mechanisms of Pb-free solder joints.

# 1. Introduction

Lead (Pb)-containing solders have been used extensively in microelectronic applications to form electrical interconnections between packaging levels, to facilitate heat dissipation from active devices, to provide mechanical/physical support, and to serve as a solderable surface finish layer on printed circuit boards (PCBs) and lead frames. However, the recent trends of worldwide environmental legislation for toxic materials and consumer demand for "green" products are accelerating the transition from Pb-containing solders to Pb-free solders in the electronic industry, although the Pb metal used for electronic solders is reported to be less than 1% of the total Pb consumption worldwide [1].

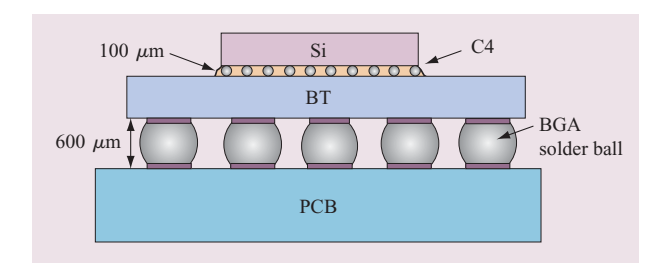
**Figure 1** shows a cross-sectional diagram of a plastic ball grid array (PBGA) package used for memory or ASIC applications. Two solder joints are highlighted; C4 (controlled collapse chip connection) solder joints, or

bumps, connecting a silicon chip to a BT-resin-based<sup>1</sup> laminate chip carrier and BGA solder joints, or balls, connecting the module to a PCB. The C4 (or flip-chip) solder joints have been used to attach flip-chips to ceramic multichip modules (MCMs) for mainframe computers or high-end servers for several decades [2]. The flip-chip has become pervasive because it provides a high-I/O-count, high-density interconnection scheme with proven performance and reliability. With respect to Pb-Sn packaging technology, the C4 solder joints used in high-performance systems are usually fabricated from Pb-rich solders such as 95Pb-5Sn or 97Pb-3Sn, while the flip-chip joints used in consumer products are fabricated from the eutectic Sn-Pb alloy, 63Sn-37Pb. In some instances, chips with 97Pb-3Sn C4 bumps are attached to the module using the 63Sn-37Pb alloy. The typical dimensions of flip-chip solder joints are of the order

©Copyright 2005 by International Business Machines Corporation. Copying in printed form for private use is permitted without payment of royalty provided that (1) each reproduction is done without alteration and (2) the Journal reference and IBM copyright notice are included on the first page. The title and abstract, but no other portions, of this paper may be copied or distributed royalty free without further permission by computer-based and other information-service systems. Permission to republish any other portion of this paper must be obtained from the Editor.

0018-8646/05/\$5.00 @ 2005 IBM

<sup>&</sup>lt;sup>1</sup>BT resin—bismaleimide triazine (polymer resin).



Schematic diagram showing a cross section of a plastic ball grid array (PBGA) package used for memory and ASIC applications.

**Table 1** Examples of Pb-free candidate solders and Pb-containing solders.

Composition (wt.%)	Melting point (°C)	Applications	Concerns
Sn-3.5Ag	221	SMT, flip-chip	Cu dissolution, excessive IMCs, voids
Sn-3.8Ag-0.7Cu	217	SMT, PTH, BGA	Cu dissolution, excessive IMCs, voids
Sn-3.5Ag-3Bi	208–215	SMT	Cu dissolution, fillet lift, low mp phase
Sn-0.7Cu	227	PTH, flip-chip	Cu dissolution, wetting, excessive IMCs
63Sn-37Pb	183	PTH, SMT, BGA	Pb toxicity
97Pb-3Sn	317	Flip-chip, C4	Pb toxicity

IMC: intermetallic compound; mp: melting point.

of 100  $\mu$ m in diameter and 200  $\mu$ m or less in pitch. Since C4 or flip-chip solder joints provide an area array connection, they yield the highest chip interconnection density compared with other interconnection schemes, such as wire bonding or tape automated bonding (TAB), which provides mainly peripheral interconnections to a chip. BGA solder joints, which also consist of an area array interconnection scheme, are usually employed to assemble plastic or ceramic modules on a PCB [3, 4]. The composition of solder balls used for PBGA modules is normally eutectic 63Sn–37Pb, while a high-Pb composition such as 90Pb–10Sn is used for ceramic BGAs (CBGAs). The BGA solder balls, with typical dimensions of the order of 600 to 900  $\mu$ m in diameter, are joined to a

module or substrate by reflowing the eutectic 63Sn-37Pb solder paste deposited onto a substrate [3, 4].

Owing to the extensive search for Pb-free solder alloys in recent years [5–9], several promising candidates have been identified for different soldering applications, with a few examples listed in Table 1. Two major Pb-containing solders, eutectic 63Sn-37Pb and Pb-rich solders used for SMT and C4 solder bumps, are also included in Table 1. It is noteworthy that most of the candidate Pb-free solders are Sn-rich, typically containing more than 90% Sn. This suggests that the physical, chemical, and mechanical properties of the proposed Pb-free solders are heavily influenced by the properties of pure Sn, in contrast to Sn-Pb eutectic, which comprises a mixture of Sn-rich and Pb-rich phases. Pure Sn is polymorphic, capable of existing as three crystal structures  $(\alpha, \beta, \gamma)$ depending on temperature and pressure [10]. Since the white tin phase ( $\beta$ –Sn) has a body-centered tetragonal (BCT) crystal structure in contrast to the face-centered cubic (FCC) structure of Pb, the physical and mechanical properties of white tin are less isotropic than those of Pb. Because of its restricted symmetry in crystal structure, white Sn is more difficult to mechanically deform than Pb. The white Sn crystal is optically birefringent, meaning that an incident polarized light beam on a  $\beta$ -Sn crystal causes the plane of polarization to rotate upon reflection. The degree of rotation is highly dependent on the crystallographic orientation of the reflecting surface. Accordingly, polarized light microscopy can be used to distinguish the orientation of  $\beta$ -Sn dendrite structures in Pb-free solders, as discussed later.

The melting point of most Pb-free commercial solders is within the range from 208°C to 227°C, which is about 30°C higher than the melting point of eutectic Sn-Pb, 183°C. The higher melting point, or reflow temperature, has serious implications for the performance of packaging materials and assembly processes, and can affect the integrity and/or reliability of Pb-free microelectronic packages. Another important issue associated with the proposed Pb-free solders is the difficulty of maintaining the type of solder melting-point hierarchy that is well established for Pb-containing solders. For example, since the melting point of Pb-rich solders for C4 solder bumps is separated by more than 100°C from the melting point of eutectic Sn-Pb used in the next level of assembly, the C4 solder joints formed at a higher temperature (e.g., 350°C) do not become molten during the subsequent eutectic Sn-Pb card assembly reflow operation (e.g., 215°C). However, the proposed Pb-free solders allow a maximum possible separation of less than 30°C between the melting points of any two solders. Hence, the process control, during successive multiple soldering processes with Pb-free solders, becomes more challenging, and its

impact on solder-joint and package reliability is not yet well understood.

Among the several Pb-free candidate solders, the near-ternary eutectic Sn–Ag–Cu (SAC) alloy compositions, which have melting temperatures around 217°C, are becoming consensus candidates [8, 9], especially for SMT card assembly, including BGA solder joints. Accordingly, extensive research and development activities are currently focused on the Sn–Ag–Cu system in order to understand the fundamental issues and to evaluate the reliability risk factors associated with solder joints formed from this alloy family, compared with the well-established Pb-containing solder joints. An in-depth review on Sn–Ag, Sn–Ag–X, and Sn–Cu solders and solder joints can be found in a recent publication [11, 12].

The present paper discusses some key aspects of Pb-free solders and solder joints not covered by earlier publications, in order to provide a better understanding of the physical metallurgy fundamentals, and reliability assessment of the risk factors associated with Pb-free solders. The topics discussed include the microstructure of Sn–Ag–Cu alloys, control of large Ag<sub>3</sub>Sn plate formation, optimization of Sn–Ag–Cu alloy composition, mechanical properties of Sn-rich solders, thermal-fatigue properties of Pb-free vs. Sn–Pb solder joints, fatigue failure mechanisms of SAC vs. Sn–Pb solder joints, interfacial reactions of Pb-free solders, spalling behavior of intermetallic compounds (IMCs), and other reliability issues associated with Pb-free solder interconnects.

# 2. Microstructures of Pb-free solder joints

#### Microstructures of eutectic solders

As listed in Table 1, most Pb-free candidate solders have either a binary or ternary eutectic composition, since a eutectic composition provides the benefit of an alloy with the lowest melting temperature of all alloys comprising the system, and it melts at a single temperature upon heating (but not during solidification). This is also true of eutectic Sn-Pb solder, whose melting temperature is 183°C. A typical microstructure of eutectic Sn-Pb solder joints found in CBGA modules is a simple mixture of two phases; a Pb-rich (dark contrast) and Sn-rich (bright contrast) phase, as noted in Figure 2. The volume fraction of each phase is proportional to the alloy composition, while the size (or spacing) of each phase is determined by the processing (or solidification) condition of solder joints; rapid heat removal during solidification generally produces a finer microstructure. The microstructural features (referred to as its morphology) of a eutectic solder, such as volume fraction, distribution, and size or spacing of each phase, determine the mechanical and physical properties of a solder joint.



Figure 2

Microstructure of eutectic Sn–Pb BGA solder joint processed at a cooling rate of about  $1^{\circ}\text{C/s}$  and thermal fatigue tested between  $-40^{\circ}\text{C}$  and  $125^{\circ}\text{C}$ .

For the ternary eutectic Sn-3.5Ag-0.9Cu [13], an equilibrium microstructure is expected to be a mixture of three phases— $\beta$ -Sn, Ag<sub>3</sub>Sn, and Cu<sub>6</sub>Sn<sub>5</sub>—and to have weight or volume ratios consistent with the eutectic composition. However, a typical microstructure observed in a Sn-3.8Ag-0.7Cu BGA joint (Figure 3) is not an equilibrium microstructure, but rather a group of complex Sn dendritic arm structures surrounded by a network in which all three phases are interspersed. In addition, depending on its cooling rate and composition, large pro-eutectic Ag<sub>3</sub>Sn plates and/or Cu<sub>6</sub>Sn<sub>5</sub> rods may also be found. The formation of this dendritic microstructure is an indication of non-equilibrium solidification during the solder joint formation. The excessive growth of large pro-eutectic phases is attributable to the fact that pure Sn or Sn-rich solders require a large amount of undercooling before the Sn phase nucleates and solidifies [14-16], while pure Pb or Pb-rich solders require a relatively small amount of undercooling, as noted in Table 2. A large amount of undercooling required to achieve solidification suggests a difficulty in nucleating solid Sn crystals within a liquid solder. This is also consistent with the observation of only a few large (several hundred microns in diameter)  $\beta$ -Sn grains within a SAC BGA solder joint [17].

The ternary phase microstructure in the inter-dendritic regions consists of fine particles of  $Ag_3Sn$  and  $Cu_6Sn_5$  in a matrix of  $\beta$ –Sn. These regions where all three phases are present surround regions of essentially pure Sn. The pure  $\beta$ –Sn regions represent single-dendrite arm structures. The three-phase regions represent the impingement zones for the growth of the neighboring  $\beta$ -Sn dendritic arm structures and are formed in the final stages of solidification. During solidification at a moderate



Microstructure of near-ternary eutectic Sn-3.8Ag-0.7Cu BGA solder joint processed at a slow cooling rate (approximately 0.5°C/s). (Courtesy of T. K. Hwang.)

**Table 2** Undercooling required for the solidification of  $\beta$ -Sn in Sn-rich and Sn-Pb solders.

Solder composition (wt.%)	Melting temp. during heating, T1 (°C)	Peak temp. during cooling, T2 (°C)	Required undercooling, $\Delta T (T1 - T2)$ (°C)
Sn-3.8Ag- 0.7Cu (SAC)	217.0	187.2	29.8
SAC + 0.1Zn	217.7	213.3	4.4
SAC + 0.7Zn	217.2	213.6	3.6
Sn-8Zn-3Bi	193.7	191.8	1.9
100Sn	232.6	217.5	15.1
95Pb-5Sn	305.6	302.4	3.2
100Pb	328.5	324.1	4.4

cooling rate, such as  $1^{\circ}$ C/s, the pro-eutectic phases of Ag<sub>3</sub>Sn plates or Cu<sub>6</sub>Sn<sub>5</sub> rods can grow to large sizes within an undercooled liquid before nucleation of the  $\beta$ -Sn phase and before the final solidification of the

ternary interdendritic microstructure, as shown in **Figure 4**. The growth of large pro-eutectic phases can be reduced kinetically by a rapid cooling rate [14, 15] and thermodynamically by reducing Ag or Cu content [15, 16]. Once the pro-eutectic phases form, they deplete Ag and Cu atoms from the surrounding Sn-rich liquid phase, and the composition of the remaining liquid locally deviates from its initial composition. This further prevents an equilibrium solidification of the ternary eutectic microstructure. The microstructures of near-eutectic ternary SAC alloys are significantly influenced by the cooling rate during reflow, and thus their mechanical and other physical properties are significantly influenced by the cooling rate [14–16].

# Effects of cooling rate

The SMT or BGA solder joints (as-joined condition) generally have the characteristics of a rapidly solidified microstructure, since the solder volume is normally small and the joints are thermally well connected to dissipate the latent heat released during the solidification process. The microstructure of solder joints is significantly influenced by reflow conditions such as peak temperature, cooling rate, solder volume, package and substrate size, and by other factors. The microstructure that results is affected by the nucleation and growth phenomena of constituent phases.

Figure 5 shows an example of the microstructure of SAC (Sn-3.8Ag-0.7Cu) BGA solder balls solidified at two different cooling rates: (a) a very rapid cooling rate (approximately 100°C/s) in an oil medium, and (b) a very slow cooling rate (0.02°C/s) in an air oven. In the rapidly cooled SAC BGA solder ball [Figure 5(a)], the fine, primary  $\beta$ -Sn dendrite structure is well developed, and the ternary microstructure is solidified in the interdendritic region; no pro-eutectic phases are noted. In the very slowly cooled solder ball [Figure 5(b)], the dendrite structure is coarsened into a rather large round shape. The spacing between the ternary phase structures becomes coarser compared with the rapidly cooled structure, because of the reduced Ag and Cu content and because of a slow rate of heat removal during the solidification process. A more rapid rate of heat removal increases the thermal gradients at the dendritic growth fronts and gives rise to finer dendritic branching. Since the eutectic structure containing the hard dispersion of Ag<sub>3</sub>Sn or Cu<sub>5</sub>Sn<sub>5</sub> is the major hardening agent of the ternary alloys, a high strength and high resistance to creep deformation are expected with the fine microstructure of the rapidly cooled solder shown in Figure 5(a). In addition, large pro-eutectic Ag<sub>3</sub>Sn or Cu<sub>6</sub>Sn<sub>5</sub> precipitates are commonly observed in the slowly cooled microstructure shown in Figure 5(b). The growth of the large Ag<sub>3</sub>Sn plate and Cu<sub>6</sub>Sn<sub>5</sub> rod structures in the

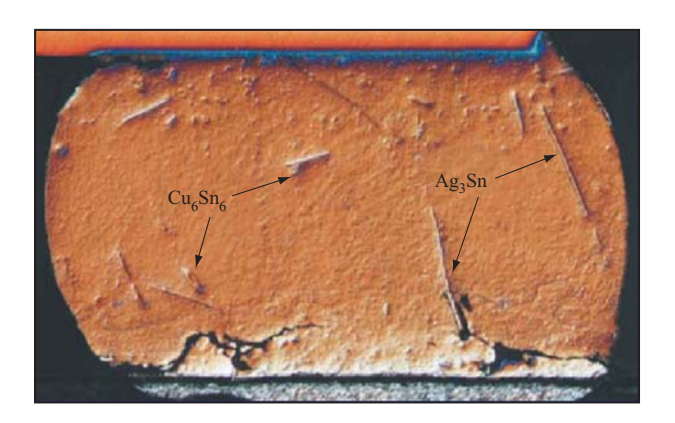


Figure 4

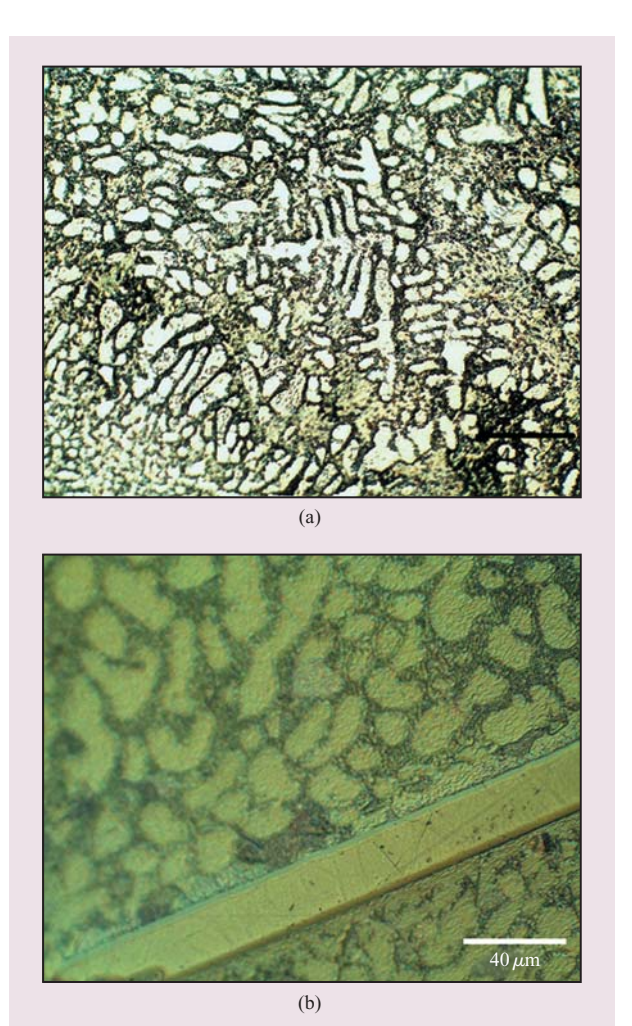
Microstructure of Sn-3.8Ag-0.7Cu BGA solder joint processed at a cooling rate of about  $1^{\circ}$ C/s and thermal fatigue tested between  $-40^{\circ}$ C and  $125^{\circ}$ C.

early stages of solidification, associated with slow cooling, diminishes the quantities of these constituents that can be incorporated in the inter-dendritic zones, thus reducing the dispersion-hardening effects of the inter-dendritic zones.

Thus, moderate or slow cooling rates have a significant effect on the microstructure of SAC alloys, forming large, pro-eutectic Ag<sub>3</sub>Sn plates [14-16]. The growth of such plates can be suppressed by employing a rapid cooling rate, such as 1.5°C/s or higher, during a reflow process of solder joints. However, providing a rapid cooling rate is not always practical, especially with substrates that have a large thermal mass. The rapid-cooling-rate operation can also produce some unwanted side effects, such as thermal stress or strain in a substrate or package. Hence, a rapid-cooling-rate process is not recommended for controlling the microstructure of SAC solder joints. As discussed in the next section, it was found that reducing Ag content in SAC alloys was a more effective and practical means of controlling the formation of large Ag<sub>3</sub>Sn plates.

#### Effects of alloying elements

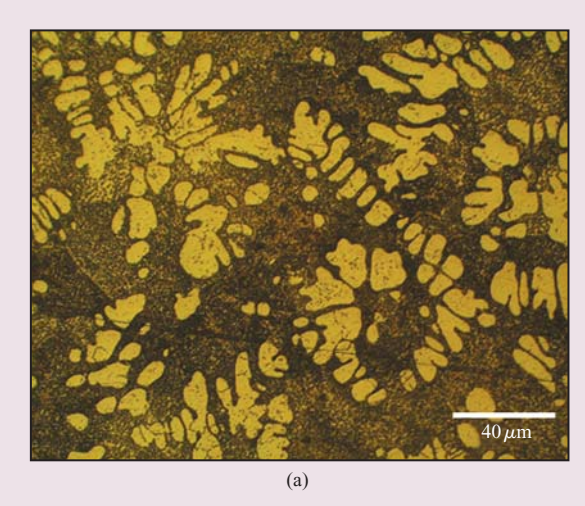
The microstructure of Sn-rich eutectic solders is strongly influenced by alloying elements, such as Ag, Cu, Sb, Bi, In, Zn, and Co. For example, the dendritic growth of the primary  $\beta$ –Sn crystal structure is quite common in binary or ternary Sn-rich solders such as Sn–0.7Cu, Sn–3.5Ag, and Sn–3.8Ag–0.7Cu, while a dendritic structure is difficult to observe in pure Sn, after solidification, because the dendrite arm impingement zones are not decorated [19]. However, the growth of Sn dendrites in a pure Sn system has been directly observed.

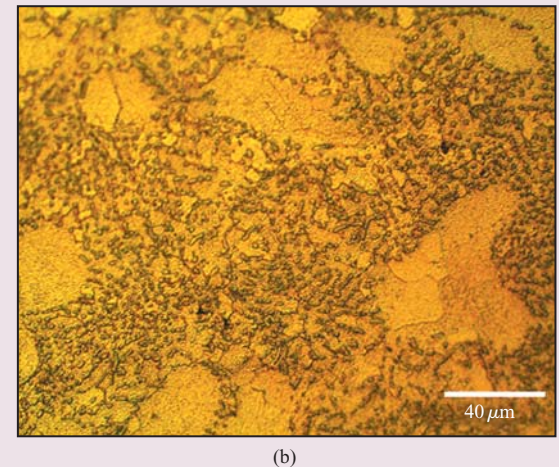


#### Figure 5

Microstructure of SAC BGA solder balls solidified at (a) very fast cooling rate, such as  $100^{\circ}\text{C/s}$ ; (b) very slow cooling rate  $(0.02^{\circ}\text{C/s})$ . Reproduced from [18] with permission.

The effects of Ag content in near-ternary eutectic SAC alloys were investigated for Ag content ranging from 3.8% to 2.0% [14–16]. For Ag content between 2.0 and 3.8 wt.%, the melting point and the amount of undercooling of SAC alloys essentially remained the same as for the ternary eutectic. Under an intermediate cooling rate of 1°C/s, the pro-eutectic Ag<sub>3</sub>Sn phase can easily grow into large plates for Ag contents higher than 3 wt.%. When the Ag content is less than 3 wt.%, the formation of large Ag<sub>3</sub>Sn plates is substantially reduced even under extremely slow cooling conditions, such as  $0.02^{\circ}$ C/s. The  $\beta$ –Sn dendrites and ternary eutectic structure appear to become finer as Ag content increases. The microstructural effect is probably derived from the effects of the growth-induced compositional gradients at the dendrite growth





Microstructure of SAC + 0.7Zn BGA solder balls solidified at (a) very fast cooling rate (100°C/s); (b) very slow cooling rate (0.02°C/s). Reproduced from [18] with permission.

fronts and their effect on dendrite branching. Both the fine dendrite and finer ternary phase structures provide a higher microhardness value compared with a coarse microstructure. A higher hardness usually means less ductility and therefore shorter thermal fatigue life; accordingly, SAC alloys with less than 3 wt.% were recommended in terms of their microstructure and mechanical properties [14–16].

A similar conclusion was reached in a study of tensile properties of near-ternary eutectic SAC alloys, where the strength of the alloys was found to depend strongly on the area fraction of the ternary phase network and the dispersion morphology of fine Ag<sub>3</sub>Sn in that eutectic network [20]. Although a ternary alloy close to the true eutectic composition had the highest strength, it had a

propensity to form large  $Ag_3Sn$  plates. Consequently, a ternary SAC alloy of Sn-3.0Ag-0.5Cu was recommended as the optimum alloy, with the lowest Ag and Cu content among the SAC alloys investigated [20].

The effects of Cu content on microstructure were investigated in near-ternary eutectic SAC solders [21, 22]. It was determined that the pro-eutectic phase formed in Sn-3.6Ag-1.0Cu is Cu<sub>6</sub>Sn<sub>5</sub>, which is consistent with the ternary phase diagram of the initial solder alloy composition. In a study of mechanical properties of Sn-Ag-Cu alloys [23], the effect of Cu content was investigated by systematically varying Cu content from 0.2 to 0.7 wt.%. It was found that the microstructure was likely to produce a dendritic growth of  $\beta$ -Sn as the Cu content increased. The effect of Cu content on the formation of the primary Ag<sub>3</sub>Sn phase was also investigated [15]. The presence of Cu in the solder appears to promote the formation of large Ag<sub>3</sub>Sn plates in the early stages of solidification, possibly by assisting the nucleation of these plates. Another important effect of Cu content reported is on the pasty range of SAC solder joints [15]. (The pasty range is defined as the difference between the liquidus and solidus temperature of a given alloy composition. It is desirable to have the smallest pasty range possible to reduce the defect rate in solder joints.) The pasty range of SAC solder joints is quite sensitive to Cu content above the eutectic composition, but not to Ag content. For Ag content ranging from 2.1% to 2.7%, the pasty range is estimated to be 2°C to 4°C for 0.7%Cu and 15°C to 17°C for 0.9%Cu. In comparing the microstructure of Sn-3.5%Ag [24] with those of the neareutectic ternary SAC alloys [23], it is noted that the presence of Cu in SAC alloys promotes more dendritic growth of  $\beta$ -Sn.

The effect of adding Zn to SAC to control the formation of large  $Ag_3Sn$  plates was investigated [18, 25]. It was also reported that Zn additions modified the microstructure of the  $\beta$ –Sn dendrite as well as the ternary eutectic microstructure. **Figure 6** shows a microstructure of SAC (Sn–3.8Ag–0.7Cu) with 0.7 wt.% Zn in which no large  $Ag_3Sn$  plates were observed, even at a very slow cooling rate. In addition, the matrix microstructures of both  $\beta$ –Sn dendrites and eutectic structure were significantly modified in comparison to the corresponding SAC without Zn addition. The effect of Zn addition on the microstructural modification of SAC joints was explained by the reduction of undercooling required for the solidification of  $\beta$ –Sn dendrites, as noted in Table 2 [18].

An addition of minor alloying elements of Co and Fe to SAC [22] was found to control the matrix microstructure by producing more ternary phase regions. This addition also suppresses the interfacial reactions on Cu substrates and is discussed in more detail later, in the

section on interfacial reactions in Pb-free solder joints during solder reflow.

# 3. Mechanical properties of Pb-free solders and joints

Several Pb-free solder alloys have been investigated in order to understand the microstructure-property relations in terms of alloying composition, plastic deformation, and annealing condition [19]. The microstructure of as-cast Sn-rich solder alloys is strongly influenced by alloying elements (Ag, Cu, or others). The Sn dendrite structure is commonly observed in binary or ternary Snrich alloys. The strain hardening of Sn-rich solders is also affected by the amount of alloying elements and degree of plastic deformation. More plastic deformation and higher alloying additions result in more hardening in Sn-rich solders, but not much hardening is observed with pure Sn. This is consistent with the recrystallization and graingrowth process of pure Sn observed during deformation at room temperature. The recrystallization and graingrowth processes occur in deformed and annealed Sn-rich solders, depending on plastic deformation and annealing conditions. Pure Sn undergoes recrystallization and grain growth even at room temperature during plastic deformation, while Sn-0.7Cu recrystallizes after annealing at 150°C for 48 hr, with a small amount of deformation (e.g., 20% or less). For Sn-3.5Ag and Sn-3.5Ag-0.7Cu, considerable deformation (30% or higher) is required for recrystallization during annealing at 150°C for 48 hr. Accordingly, it is found that Sn-3.5Ag-0.7Cu has the highest microstructural stability during deformation and annealing among the leading Pb-free solder candidate alloys.

Figure 7 compares the microhardness of several Pb-free solders with eutectic Sn-37Pb solder as a function of testing temperature. The solder samples were prepared as pellets measuring 5.1 mm (0.200 in.) in diameter and 3.2 mm (0.125 in.) in height, solidified in a graphite mold at a cooling rate of 4°C/s [19]. The microhardness was measured at an elevated temperature between 25°C and 130°C by heating a polished pellet sample on a solid-state heater attached to a platform of a microhardness tester. The Vickers hardness number (VHN) reported is an average value of ten indentations made on each pellet using a 50-g load. The room-temperature hardness value is in good agreement with the results reported previously [19]. Sn-3.5Ag-0.7Cu has the highest hardness among the solders tested, regardless of test temperature. Sn-37Pb is slightly lower than Sn-3.5Ag-0.7Cu in hardness, and pure Sn exhibits the lowest hardness at all test temperatures. As the test temperature increases from 25°C to 130°C, there is a trend of gradual reduction in hardness for each solder composition. At 130°C, both Sn-3.5Ag-0.7Cu and Sn-37Pb exhibit about the same

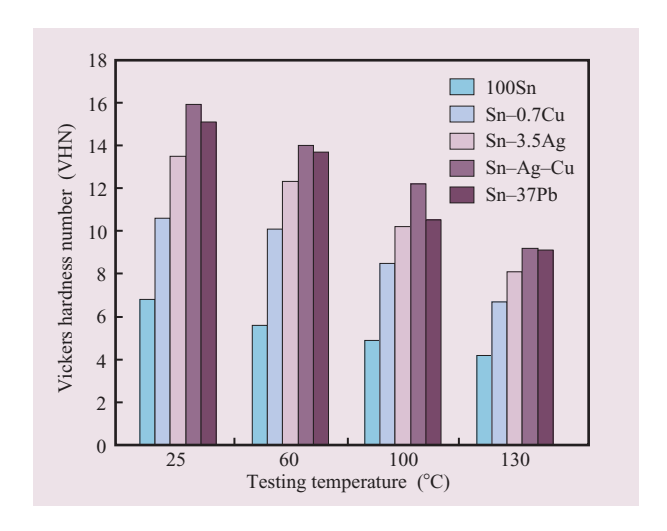


Figure 7

Vickers microhardness numbers of Pb-free and Sn–Pb solders as a function of testing temperature. Solders were solidified at  $4.0^{\circ}$ C/s, and the testing was conducted using 50-g load.

hardness, suggesting that the hardness reduction is greater for Sn-3.5Ag-0.7Cu than eutectic Sn-Pb.

The mechanical and electrical properties of Pb-free solder joints, fabricated from three solder alloys (Sn-3.5Ag, Sn-3.5Ag-0.7Cu, and Sn-3.5Ag-4.8Bi) and two surface finishes [Cu and Au/Ni(P)], were evaluated in terms of reflow time, IMC thickness, and morphology [26]. The shear strength of Pb-free solder joints on a Cu surface finish is not significantly affected by the reflow time or IMC thickness. However, when IMCs occupy approximately two thirds of a joint gap, there is a significant reduction in the shear strength in the case of Cu. The shear strength of Au/Ni(P) joints is much lower than that of Cu joints and decreases steadily with reflow time or increased IMC thickness. The electrical resistance of Pb-free solder joints increases initially and then decreases for an extended reflow or aging time for both Cu and Au/Ni(P). This trend was explained in term of the growth behavior of IMCs in the solder joint [26]. For an extended reflow time, a large Ag<sub>3</sub>Sn plate can short two interfaces, resulting in a reduction of the electrical resistance of the joint.

Mechanical properties are much more difficult to determine for solder joints than for bulk solders. For a given solder composition, many variables, such as joint geometry, solder volume, and joining process, affect solder joint properties. **Table 3** compares the shear-strength measurements reported for several Pb-free solder joints. For example, the shear strength of Sn–3.8Ag–0.7Cu joints has a wide range from 12.5 to 47 MPa, depending on strain rate, solder-joint gap, and test

**Table 3** Shear strength of Pb-free solder joints (to Cu substrate).

Solder alloy (wt.%)	Test method				
	Ring and plug shear strength (MPa)	Four-point bend shear strength (MPa)	Flip-chip shear strength (MPa)	Lap-joint shear strength (MPa)	
63Sn-37Pb	32.7	29	9.2	50	
Sn-3.65Ag	37.2 (Sn-3.5Ag)	28	11.4 (Sn-3.5Ag)	38	
Sn-0.7Cu	27.0		9.2		
Sn-3.8Ag-0.7Cu	35.1	47 (3.6Ag–1Cu)	12.5	39	
Sn-3.5Ag-3Bi				49.6	
Parameters					
Strain rate (mm/min)	0.10	0.10	15	0.25	
Solder-joint gap (mm)	175	76	100	20	
Reference	C. Foley et al. [27]	B. A. Cook et al. [28]	D. R. Frear et al. [29]	S. K. Kang et al. [26]	

method. This clearly demonstrates that care must be exercised in utilizing data reported in the literature.

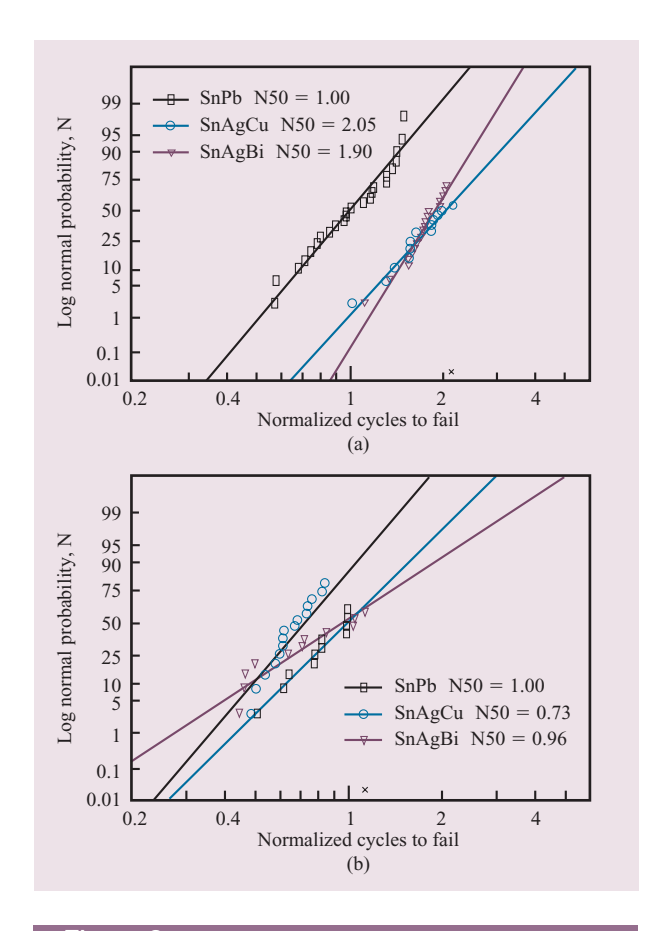
In addition, it was recently reported that traditional mechanical testing conducted at a slow strain rate in conjunction with lap shear or ball shear tests may not provide adequate information regarding the joint integrity or impact reliability of solder joints. This subject is discussed further in Section 5.

# 4. Thermal-fatigue properties of Pb-free vs. Pb-containing solder joints

Good thermal-fatigue life of solder joints is a critical reliability requirement for high-performance microelectronic systems, in which solder joints provide electrical and thermal paths in addition to physical support. Thermal-fatigue behavior of selected Pb-free BGA solder joints (Sn-3.8Ag-0.7Cu and Sn-3.5Ag-3.0Bi) was investigated in comparison with conventional eutectic Sn-Pb joints using ceramic BGA modules attached to an organic card [30]. It was determined that the thermal-fatigue behavior of Pb-free solder joints is dramatically more sensitive to the choice of accelerated thermal cycle (ATC) temperature range and peak temperature than eutectic Sn-Pb controls. Figure 8 compares the thermal-fatigue behavior of Pb-free solder joints on a 625-I/O CBGA (module size 32 mm by 32 mm by 0.8 mm) with eutectic Sn-Pb, exposed to ATC test conditions. For 0°C to 100°C ATC testing (30-min cycle), the thermal-fatigue performance of two Pb-free solder joints, Sn-3.8Ag-0.7Cu and Sn-3.5Ag-3.0Bi, was determined to be superior to that of the eutectic Sn-Pb control alloy, as shown in Figure 8(a). For -40°C to 125°C ATC testing (240-min cycle), both Sn-3.8Ag-0.7Cu and Sn-3.5Ag-3.0Bi were inferior to the eutectic Sn-Pb, indicating the sensitivity of ATC test conditions with Pb-free solder joints, as shown in Figure 8(b). In further experiments, high peak temperatures such as 125°C were determined to have a significant effect on reducing fatigue resistance, but this effect was not observed at low peak temperatures. This observation is consistent with other mechanical behaviors of Pb-free solders at an elevated temperature, such as creep sensitivity and the high-temperature hardness data discussed earlier.

Thermal fatigue behavior of SAC solder joints was also investigated in terms of Ag content, in particular to assess any beneficial effects of a low Ag content in SAC alloy (for example, the reduction of large Ag<sub>3</sub>Sn plate formation) [31, 32]. The Ag content in BGA solder balls was investigated in the range from 2.1% to 3.8%. Two different cooling rates (0.5°C/s vs. 1.7°C/s) during reflow were used to control the joint microstructure. Three ATC test conditions were chosen, with two temperature ranges (0°C to 100°C and -40°C to 125°C) and two thermal cycle frequencies (30 min and 120 min). The low-Ag joints (Sn-2.1Ag-0.9Cu) assembled at the slow cooling rate (0.5°C/s) exhibited the best thermal-fatigue life compared with high-Ag joints tested at 0°C to 100°C ATC with a 120-min cycle time. The thermal-fatigue life of low-Ag-content solder alloys was determined to be less dependent on cooling rate than that of high-Ag joints. The high-Ag joints (Sn-3.8Ag-0.7Cu) assembled at 0.5°C/s exhibit the best thermal fatigue life of all the joints for the 0°C to 100°C ATC with a 30-min cycle time. A slow cooling rate is beneficial for enhanced thermal-fatigue resistance

614



Thermal fatigue behavior of Pb-free BGA solder joints and eutectic Sn–Pb in ATC testing at (a)  $0^{\circ}$ C to  $100^{\circ}$ C, 30-min cycle time; (b)  $-40^{\circ}$ C to  $125^{\circ}$ C, 240-min cycle time. Reproduced from [30] with permission.

regardless of Ag content or ATC test condition. The fatigue crack propagation pattern in high-Ag joints is more or less confined to the near-pad-interface region, while in low-Ag joints the crack propagation is well within the solder joint, suggesting a greater ductility for the low-Ag joints compared with high-Ag joints. The role of large Ag<sub>3</sub>Sn plates with respect to fatigue life is found to be a complex issue, being detrimental when the plates are aligned in the direction of crack propagation. In light of this effect, the presence of the plates is certainly not desirable, and it is strongly recommended that the growth of large Ag<sub>3</sub>Sn plates be suppressed in order to reduce the reliability risk factor for SAC joints [31, 32].

On the basis of extensive failure analysis of ATC samples of Sn-Ag-Cu CBGA solder joints in comparison with eutectic Sn-Pb joints, the fatigue crack propagation mechanisms are found to be very different. In the Sn-Pb samples, because of accumulated strains at the interface and repeated exposure to elevated temperatures during

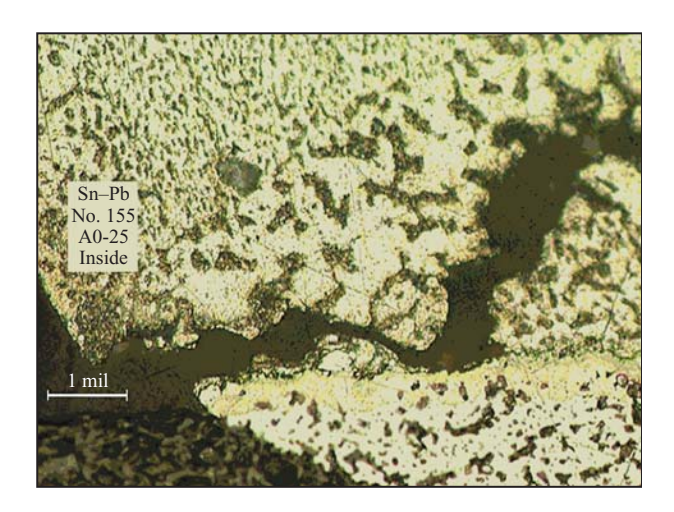


### Figure 9

Thermal-fatigue crack propagation in eutectic Sn–Pb solder joints in a CBGA module (ATC testing from 0°C to 100°C, 30-min cycle).

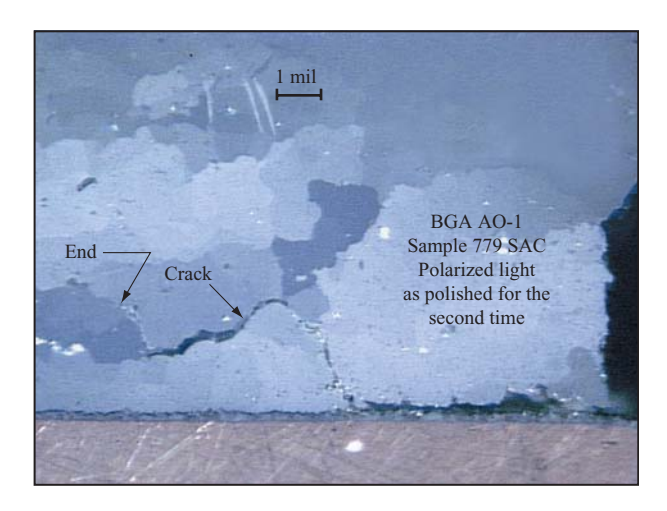


# Figure 10

Thermal-fatigue crack propagation in Sn-3.8Ag-0.7Cu joints in a CBGA module (ATC testing from -40°C to 125°C, 42-min cycle). Reproduced from [17] with permission.

ATC, microstructural coarsening of the Sn and Pb phases occurs near the failing interface, as shown in **Figure 9**. This causes localized softening near the interface and eventually provides an easy path for fatigue crack propagation. This process has been well known for eutectic Sn–Pb joints [33]. In the case of Sn–Ag–Cu solder, under cyclic thermomechanical deformation, the  $\beta$ -Sn phase is observed to recrystallize dynamically in regions of high plastic deformation, specifically near the pad interfaces, as shown in **Figure 10**. The recrystallized

regions of fine grains are also expected to be more susceptible to creep deformation (such as grain boundary sliding or cracking) than the initial microstructure. Hence, the recrystallized region provides an easy path for crack propagation during ATC and shortens the thermal-fatigue life [17].

The thermal-fatigue behavior of flip-chip joints is much more complex to evaluate than that of BGA joints; in addition to being affected by the choice of solder alloy composition and under-bump metallurgy (UBM), it is also affected by the bump deposition process, underfill materials, ATC test conditions, and others. In addition, because of the small volume of a flip-chip solder bump, the role of the solder/UBM interfacial reaction becomes critical in determining the thermal-fatigue failure mechanisms. Hence, not many investigations on the thermal fatigue of Pb-free flip-chip joints have been reported so far. As a screening test, isothermal mechanical testing under a strain-controlled condition was conducted with several Pb-free flip-chip solder bumps produced using stencil-printed solder pastes, without underfill encapsulation [29]. The Sn-0.7Cu on both Cu and Ni UBM exhibited the best mechanical-fatigue life of all of the solder/UBM systems evaluated, including eutectic Sn-Pb [29]. In a subsequent study, a thermomechanicalfatigue test (0°C to 100°C) was conducted with the same solder/UBM systems without underfill encapsulation. The Sn-0.7Cu joints again exhibited the best thermal-fatigue life [34]. The thermal-fatigue failure mode of Sn-0.7Cu flip-chip is massive solder deformation without involving the brittle solder/intermetallic interface. This may well account for the fact that Sn-0.7Cu alloy performed the best in thermal-fatigue testing among the solders investigated [34]. In a recent study, excellent thermalfatigue life of electroplated Sn-0.7Cu flip-chip bumps with underfill encapsulation was reported: 5,322 cycles for Cu UBM tested at −55°C to 150°C, and 6,588 cycles for Ni UBM tested at -40°C to 125°C [35]. In addition, no electromigration failure was observed with several Pb-free solder joints when they were tested at up to  $2.55 \times 10^4$  A/cm<sup>2</sup> at 150°C for 2,338 hr [36].

By using commercially available electroplated SnAg bumps with Ti/Cu/Ni UBM, a Pb-free flip-chip package was qualified for chip assembly process [37]. Several reliability tests were conducted, including thermal cycling, high-temperature storage, and electromigration. The ATC testing was performed (–55°C to 125°C, two cycles per hour), and the bump structure was observed not to degrade appreciably up to 1,500 cycles. It was also demonstrated that the electromigration lifetime was longer by more than an order of magnitude in comparison with eutectic Sn–Pb bumps at a constant-current stress up to 800 mA at temperatures up to 165°C [37].

#### 5. Interfacial reactions in Pb-free solder joints

#### During solder reflow

The interfacial reaction between molten solder and a surface finish on a PCB or UBM in a flip-chip is essential to provide proper wetting of the solder, to achieve a metallurgical bond at the joint, and to provide necessary joint strength. However, excessive interfacial reactions can cause poor joint strength and degrade the long-term reliability of solder joints. Several interfacial reactions have been identified during soldering, such as dissolution of a surface finish layer into a molten solder [38–40], concurrent formation of intermetallic compounds (IMCs) at the interface [40-42], and spalling (or separation) of IMCs [43-45]. When interfacial reactions are likely to be excessive, a reaction (or diffusion) barrier layer such as a Ni layer (electroplated or electroless) is employed over the Cu base metal to control its dissolution and IMC growth. Interfacial reactions can continue in the solid state during thermal exposure, when testing or in service. However, the kinetics of reaction in the solid state are much slower than the liquid state.

In Pb-free solder joints, the interfacial reactions are known to be more severe (rapid and copious) than in eutectic Sn–Pb, because of their high Sn content and high reflow temperature. In general, Sn-rich Pb-free solders exhibit faster kinetics of Cu or Ni dissolution and IMC growth than eutectic Sn–Pb [38, 39]. Numerous investigations with Pb-free solders have recently been conducted to understand the mechanisms of their interfacial reactions. Several important factors identified include solder composition [38, 39], minor alloying elements [21, 22], ratio of solder volume to solder pad area [41], diffusion barrier layer (thickness, deposition method) [42, 43], solder application method (paste vs. plating) [39, 43], and reflow conditions [40].

Since the molten Sn is the most active metal to react with the surface finish layer during reflow, the amount of base metal dissolution and IMC growth are strong functions of the Sn content of a solder, reflow temperature, and time. It is interesting to note that a small addition of alloying elements such as Cu, Ni, Fe, and Co can significantly change the characteristics of IMC growth [21, 22]. In a study involving the reaction between pure Sn and Cu or Ni, it was demonstrated that IMC growth is significantly affected by the ratio of solder volume to solder pad area, which determines the total amount of base metal to be dissolved at a given reflow temperature [41, 42].

The nature of a diffusion barrier layer, such as electroless vs. electroplated Ni, also determines their interfacial reactions; electroplated Ni generally dissolves and reacts more slowly than electroless Ni into Sn-rich solders [39]. Recently, electroless Ni(P) metallization has

received great attention as a reaction barrier layer for Pb-free solder joints because of its low cost and simple processing steps. However, the interfacial reactions with Ni(P) are more complex, because of the formation of a P-rich layer between the Ni-Sn IMC and Ni(P), created during reflow and solid-state annealing [43–45]. As the interfacial reaction progresses with Ni(P), spalling of Ni-Sn IMCs from the interface is commonly observed because of the formation of P-rich compounds during reflow or annealing at an elevated temperature [43, 44]. It has also been demonstrated that the P content is a critical factor in determining the IMC spalling and formation of P-rich layers; high P content increases the propensity for IMC spalling [43]. It was also determined that the solderdeposition method (plating vs. solder paste) is important to the IMC spalling behavior. Upon reflow, solder paste reflowed causes more spalling than electroplated solder under equivalent conditions [43]. The IMC spalling from a Ni(P) layer is also closely related to the crystallization process. A Ni-Sn-P layer forms between Ni<sub>3</sub>Sn<sub>4</sub> and crystalline Ni<sub>3</sub>P, causing Ni-Sn IMC spalling to occur from the Ni-Sn-P surface [43]. The IMC spalling becomes less severe from a Ni(P) layer when Sn-rich solders contain a small amount of Cu, possibly by altering the structure or composition of Ni-Sn IMCs [39, 42, 44].

#### During annealing at elevated temperature

It was recently reported that interfacial reactions of Sn-Ag-Cu joints subjected to long-term annealing at an elevated temperature (such as 150°C) cause serious reliability concerns under impact loading conditions. This is attributed to the formation of voids between the interfacial IMCs and Cu base metal, particularly through the growth of the second IMC layer, Cu<sub>3</sub>Sn [22, 46]. The void formation may be caused by an imbalance in atomic flux across the diffusing interface; that is, Cu atoms diffuse out faster across the Cu-Sn IMC layer(s) toward the solder than Sn atoms diffuse through the IMCs from the Sn-rich solder. This phenomenon, known as the Kirkendall effect, was originally observed to occur during an interdiffusion experiment between Cu and Cu-Zn alloy, where Zn atoms diffuse more rapidly than Cu atoms across the interface [47]. Upon an extended annealing of SAC joints in contact with Cu at 150°C, voids are observed at the interface between Cu and IMCs, and with continued annealing can grow and coalescence into a void layer as the annealing time increases. This void structure can drastically reduce the joint strength of Pb-free solder joints [46]. At an early stage, however, the presence of voids is difficult to detect by conventional mechanical testing such as the lap shear or ball shear test, normally conducted at a slow strain rate. However, a drop or impact test that results in a high strain rate is reported to be effective in detecting joint strength

degradation and the presence of voids [46, 48]. The recent proliferation of mobile electronic devices that may be inadvertently dropped requires an enhanced reliability criterion for impact-related failures of Pb-free solder joints to be used in consumer electronics. Accordingly, several approaches have been proposed to improve the impact reliability of Sn-rich solder joints. Among these are the placement of a diffusion barrier layer over Cu, such as electroless Ni(P) or electroplated Ni [48]; or the addition of minor alloying elements into the SAC alloys to control the IMC growth [22, 48].

### 6. Optimization of Sn-Ag-Cu alloy composition

### Ag and Cu composition

The beneficial effects of a reduced Ag content in Sn-Ag-Cu alloys are well demonstrated in the literature [16, 31, 32], especially for Ag contents less than 3 wt.%, in minimizing the formation of large Ag<sub>3</sub>Sn plates. This situation becomes more critical when the solder volume becomes smaller, for example in flip-chip solder bumps. In electroplated Sn-Ag bumps to be used for flip-chip applications, the high Ag content has caused the growth of large Ag<sub>3</sub>Sn plates that often physically connect neighboring bumps [49]. In addition, a large volume fraction of Ag<sub>3</sub>Sn plates within a single solder bump could significantly alter the mechanical properties and thereby affect the long-term reliability of the solder joint or the reliability of the package to which it is attached. Considering the high material cost and the potential impact to the environment during the extraction of its constituent elements [50], a low Ag content is much favored over the high Ag content currently used for card assembly as a leading Pb-free solder.

The influence of Cu content on the formation of large Ag<sub>3</sub>Sn plates in Sn-Ag-Cu alloys appears less sensitive than the influence of Ag content on Ag<sub>3</sub>Sn plate formation. However, it has been shown that a high Cu content can lead to the formation of large quantities of Cu<sub>6</sub>Sn<sub>5</sub> rods, especially when Cu metallization is used in a solder joint. Additionally, a high Cu content, above the eutectic composition of 0.9 wt.% Cu, in SAC alloys increases the pasty range (the difference between the liquidus and the solidus temperature of the SAC alloy) [15]. A large pasty range may not be acceptable, because the "fillet-lifting" solder defect rate in solder joints may rise dramatically. Thus, depending on how significant the pasty range is in an intended application, it may be desirable for the Cu content in the SAC alloy to be no higher than 0.7-0.9 wt.%.

#### Tin pest

The allotropic transformation of white tin ( $\beta$ –Sn, tetragonal structure) to gray tin ( $\alpha$ –Sn, cubic structure)

617

at temperatures below 13°C to form tin pest is another serious reliability issue associated with Sn-rich, Pb-free solders. The formation of tin pest has been reported in bulk samples of Sn-0.7wt.%Cu [15, 51], but not in Sn-Ag-Cu subjected to -40°C for approximately two years, with one solder lot having been evaluated to date [15]. Since the tin pest transformation to gray tin causes a large volume change and concurrent cracking on the surface, it is desirable to modify the composition of Sn-Ag-Cu alloys in order to retard the transformation. This has been demonstrated by adding minor elements such as Bi, Sb, or Pb [52]. Combining our experimental results and information from the literature, a new series of modified Sn-Ag-Cu alloys has been proposed, of which the Sn-2.3Ag-0.5Cu-0.2Bi (wt.%) BGA alloy for card assembly using standard Sn-3.8Ag-0.7Cu solder paste is an example [53]. A small amount of Bi content in the alloy is intended to retard the gray tin transformation, as claimed in the literature. However, the thermal-fatigue life of Biadded SAC joints was not favorable compared with that of other SAC joints, possibly because of a hardening effect of Bi [31, 32].

#### Addition of minor alloying elements

A small Zn addition to SAC alloys was reported to cause a drastic reduction in the formation of large Ag<sub>3</sub>Sn plates regardless of cooling rate [16, 25]. The role of Zn additions to the SAC alloy is explained through the reduction in the amount of undercooling during the solidification of tin dendrites, which shortens the time available for the growth of large Ag<sub>3</sub>Sn plates in the cooling process. Since the Zn-modified SAC is not much affected by the cooling rate during reflow, it has a practical advantage over the standard SAC alloy, whose microstructure (especially the growth of Ag<sub>3</sub>Sn plates) is very sensitive to the cooling rate, with higher-Ag-content SAC alloys. In addition, the Zn-modified SAC alloys have different interfacial reaction characteristics with Cu and Ni metallization [18, 54]. It was also observed that a small addition of Zn (0.7 wt.%) to SAC significantly reduced the growth of a Cu<sub>3</sub>Sn IMC layer that is believed to be responsible for Kirkendall voids during the solidstate annealing of Sn-rich, Pb-free solder joints, when in contact with Cu metallization [54].

To enhance the impact reliability of Sn–Ag–Cu joints in conjunction with Cu metallization, several other minor alloying elements have been proposed, including Co, Fe, Ni, and In [21, 22, 46, 48]. Some disadvantages of adding more alloying elements into ternary SAC alloys would be expected—for example, difficulty in composition control, high-temperature melting process required for dissolution of high-temperature-melting metals, hardening of the alloys, and possible materials cost increase.

#### 7. Summary

Since the enforcement date (July 1, 2006) of the European legislation to eliminate Pb from various microelectronic applications including solders is rapidly approaching, the need to understand the fundamental issues associated with the leading Pb-free candidate solders is becoming increasingly important. A better understanding of the physical metallurgy of the Sn–Ag–Cu alloy system is critical in reducing the reliability risk factors when this solder is used in actual products. Several fundamental issues discussed in the paper include the microstructure evolution of near-ternary eutectic Sn-Ag-Cu solder joints, the factors affecting the microstructure, the microstructure-property relations, especially mechanical properties, thermal-fatigue mechanisms of Sn-Ag-Cu vs. eutectic Sn-Pb joints, and the interfacial reactions of Pbfree solders with the proposed surface finish layers on PCB or under-bump metallization in flip-chip solder bumps. Several factors affecting the thermal-fatigue reliability and impact reliability of the Sn-Ag-Cu solder joints have also been discussed. Finally, a possible solution to improve the reliability of Pb-free solder joints has been proposed by suggesting a modified alloy composition of the Sn-Ag-Cu alloy system.

#### References

- K. J. Puttlitz, in *Handbook of Lead-Free Solder Technology for Microelectronic Assemblies*, K. J. Puttlitz and K. A. Stalter, Eds., Marcel Dekker, Inc., New York, 2004, pp. 1–47.
- P. A. Totta, in *Area Array Interconnection Handbook*, K. J. Puttlitz and P. A. Totta, Eds., Kluwer Academic Publishers, The Netherlands, 2001, pp. 1–36.
- 3. M. J. Kuzawinski and T. R. Homa, Ibid., pp. 577-613.
- 4. M. S. Cole, K. J. Puttlitz, and R. Lanzone, *Ibid.*, pp. 656–701.
- NCMS Lead-Free Solder Project Final Report, National Center for Manufacturing Sciences, Ann Arbor, MI, August 1997
- P. T. Vianco and C. May, Proceedings of the Surface Mount International Conference (SMI '95), 1995, pp. 481–494.
- 7. 2002 Lead-Free Roadmap, Japan Electronics and Information Technology Industries Association (JEITA); see www.jeite.org.
- J. Bath, C. Handwerker, and E. Bradley, Circuits Assembly 11, 45–52 (2000).
- I. E. Anderson, J. C. Foley, B. A. Cook, J. Harringa, R. K. Terpstra, and O. Unal, J. Electron. Mater. 29, 1050–1059 (2001)
- J. D. Barnett, H. T. Hall, and R. B. Bennion, Science 141, No. 3585, 1041–1042 (1963).
- K. J. Puttlitz, in *Handbook of Lead-Free Solder Technology for Microelectronic Assemblies*, K. J. Puttlitz and K. A. Stalter, Eds., Marcel Dekker, Inc., New York, 2004, pp. 239–280.
- 12. S. K. Kang, Ibid., pp. 281-300.
- K. W. Moon, W. J. Boettinger, U. R. Kitten, F. S. Biancaniello, and C. A. Handwerker, J. Electron. Mater. 29, 1122–1136 (2000).
- D. W. Henderson, T. Gosselin, A. Sarkhel, S. K. Kang, W. K. Choi, D. Y. Shih, C. Goldsmith, and K. Puttlitz, *J. Mater. Res.* 17, 2775–2778 (2002).
- S. K. Kang, W. K. Choi, D. Y. Shih, D. W. Henderson, T. Gosselin, A. Sarkhel, C. Goldsmith, and K. Puttlitz, Proceedings of the 53rd Electronic Components and Technology Conference, New Orleans, May 2003, pp. 64–70.

- S. K. Kang, W. K. Choi, D. Y. Shih, D. W. Henderson, T. Gosselin, A. Sarkhel, C. Goldsmith, and K. Puttlitz, J. Minerals, Metals, & Mater. Soc. 55, No. 6, 61–65 (2003).
- D. W. Henderson, J. J. Woods, T. A. Gosselin, J. Bartelo,
   D. E. King, T. M. Korhonen, M. A. Korhonen, L. P. Lehman,
   E. J. Cotts, S. K. Kang, P. Lauro, D. Y. Shih, C. Goldsmith,
   and K. J. Puttlitz, J. Mater. Res. 19, No. 6, 1608–1612 (2004).
- S. K. Kang, D. Y. Shih, D. Leonard, D. W. Henderson, T. Gosselin, S. Cho, J. Yu, and W. K. Choi, J. Minerals, Metals, & Mater. Soc. 56, No. 6, 34–38 (2004).
- P. Lauro, S. K. Kang, W. K. Choi, and D. Y. Shih, J. Electron. Mater. 32, No. 12, 1432–1440 (2003).
- K. S. Kim, S. H. Huh, and K. Suganuma, *Mater. Sci. & Eng. A* 333, 106–114 (2002).
- I. E. Anderson, B. A. Cook, J. Harringa, and R. L. Terpstra, J. Electron. Mater. 31, 1166–1174 (2002).
- I. E. Anderson and J. L. Harringa, J. Electron. Mater. 33, 1485–1496 (2004).
- P. T. Vianco, J. A. Rejent, and J. J. Matin, J. Minerals, Metals, & Mater. Soc. 55, No. 6, 50–55 (2003).
- F. Ochoa, J. J. Williams, and N. Chawla, J. Minerals, Metals, & Mater. Soc. 55, No. 6, 56–60 (2003).
- K. L. Buckmaster, J. J. Dziedzic, M. A. Masters, B. D. Poquette, G. W. Tormoen, D. Swenson, D. W. Henderson, T. Gosselin, S. K. Kang, D. Y. Shih, and K. J. Puttlitz, presented at the TMS 2003 Fall Meeting, Chicago, November 2003; see www.tms.org.
- S. K. Kang, W. K. Choi, M. J. Yim, and D. Y. Shih, J. Electron. Mater. 31, 1292–1303 (2002).
- 27. C. Foley, A. Gickler, F. H. Leprevost, and D. Brown, *J. Electron. Mater.* **29**, 1259 (2000).
- B. A. Cook, I. Anderson, J. Harringa, R. Terpstra, J. Foley,
   O. Unal, and F. Laabs, J. Electron. Mater. 30, 1214 (2001).
- D. R. Frear, J. W. Jang, J. K. Lin, and C. Zhang, J. Minerals, Metals, & Mater. Soc. 53, No. 6, 28–32 (2001).
- J. Bartelo, S. Cain, D. Caletka, K. Darbha, T. Gosselin, D. Henderson, D. King, K. Knadle, A. Sarkhel, G. Thiel, C. Woychik, D. Y. Shih, S. K. Kang, K. Puttlitz, and J. Woods, *Proceedings of APEX 2001*, San Diego, January 14–18, 2001, LF2-2.
- S. K. Kang, P. Lauro, D. Y. Shih, D. W. Henderson, J. Bartelo, T. Gosselin, S. R. Cain, C. Goldsmith, K. Puttlitz, T. K. Hwang, and W. K. Choi, *Mater. Trans. (Jpn. Inst. Metals)* 45, No. 3, 695–702 (2004).
- 32. S. K. Kang, P. Lauro, D. Y. Shih, D. W. Henderson, T. Gosselin, J. Bartelo, S. R. Cain, C. Goldsmith, K. J. Puttlitz, and T. K. Hwang, *Proceedings of the 54th Electronic Components and Technology Conference*, May 2004, pp. 661–667.
- D. Frear, D. Grivas, and J. W. Morris, J. Electron. Mater. 17, 171–180 (1988).
- J. K. Lin, A. De Silva, D. Frear, Y. Guo, S. Hayes, J. W. Jang, L. Li, D. Mitchell, B. Yeung, and C. Zhang, *IEEE Trans. Electron. Pkg. & Manuf.* 25, 300–307 (2002).
- J. K. Lin, J. W. Jang, S. Hayes, and D. Frear, Proceedings of the 54th Electronic Components and Technology Conference, May 2004, pp. 642–649.
- J. K. Lin, J. W. Jang, and J. White, Proceedings of the 53rd Electronic Components and Technology Conference, New Orleans, May 2003, pp. 816–821.
- B. Ebersberger, R. Bauer, and L. Alexa, Proceedings of the 54th Electronic Components and Technology Conference, May 2004, pp. 683–691.
- 38. S. K. Kang, R. S. Rai, and S. Purushothaman, *J. Electron. Mater.* **25**, No. 7, 1113–1120 (1996).
- S. K. Kang, D. Y. Shih, K. Fogel, P. Lauro, M. J. Yim, G. Advocate, M. Griffin, C. Goldsmith, D. W. Henderson, T. Gosselin, D. King, J. Konrad, A. Sarkhel, and K. J. Puttlitz, *IEEE Trans. Electron. Pkg. & Manuf.* 25, No. 2, 1–7 (2002).
- 40. S. K. Kang, W. K. Choi, D. Y. Shih, P. Lauro, D. W. Henderson, T. Gosselin, and D. N. Leonard, *Proceedings of*

- the 52nd Electronic Components and Technology Conference, May 2002, pp. 147–153.
- W. K. Choi, S. K. Kang, and D. Y. Shih, J. Electron. Mater. 31, 1283–1291 (2002).
- W. K. Choi, S. K. Kang, Y. C. Sohn, and D. Y. Shih, Proceedings of the 53rd Electronic Components and Technology Conference, New Orleans, May 2003, pp. 1190–1196.
- Y. C. Sohn, J. Yu, S. K. Kang, D. Y. Shih, and T. Y. Lee, Proceedings of the 54th Electronic Components and Technology Conference, May 2004, pp. 75–81.
- W. Paik, Y. D. Jeon, and M. G. Cho, Proceedings of the 54th Electronic Components and Technology Conference, May 2004, pp. 675–682.
- K. N. Tu, A. M. Gusak, and M. Li, J. Appl. Phys. 93, No. 3, 1335–1353 (2003).
- T. C. Chiu, K. Zeng, R. Stierman, D. Edwards, and K. Ano, Proceedings of the 54th Electronic Components and Technology Conference, May 2004, pp. 1256–1262.
- E. Kirkendall, L. Thomassen, and C. Upthegrove, *Trans. AIME* 133, 186–203 (1939).
- 48. M. Date, T. Shoji, M. Fujiyoshi, K. Sato, and K. N. Tu, Proceedings of the 54th Electronic Components and Technology Conference, May 2004, pp. 668–674.
- D. Mis (Unitive, Inc.), presented at the Peaks in Packaging Conference (Semiconductor International), October 10, 2003; see www.unitive.com.
- A. Ku, O. Ogunseitan, J. D. Saphores, A. Shapiro, and J. M. Schoenung, *Proceedings of the 53rd Electronic Components and Technology Conference*, New Orleans, May 2003, pp. 47–53.
- 51. Y. Kariya, N. William, C. Gagg, and W. Plumbridge, J. Minerals, Metals, & Mater. Soc. 53, 39-41 (2001).
- W. G. Burgers and I. J. Groen, *Faraday Soc. Discuss.* 23, 183 (1957).
- D. W. Henderson, T. Gosselin, S. K. Kang, W. K. Choi, D. Y. Shih, C. Goldsmith, and K. Puttlitz, U.S. Patent 6,805,974, October 19, 2004.
- S. K. Kang, D. Y. Shih, and D. Leonard, presented at the 2005 TMS Annual Meeting, San Francisco, February 13–17, 2005; see www.tms.org.

Received October 7, 2004; accepted for publication February 16, 2005; Internet publication August 30, 2005 Sung K. Kang IBM Research Division, Thomas J. Watson Research Center, P.O. Box 218, Yorktown Heights, New York 10598 (kang@us.ibm.com). Dr. Kang is a Research Staff Member in the Electronic and Optical Packaging Department at the IBM Thomas J. Watson Research Center. He received a B.S. degree in metallurgical engineering from Seoul National University, Korea, and a Ph.D. degree in materials science and metallurgy from the University of Pennsylvania. He was a postdoctoral research fellow at Carnegie Mellon University (1973-1976), a Research Scientist at Nova Scotia Technical University, Halifax, Canada (1976–1977), an Assistant Professor at Stevens Institute of Technology (1977-1980), and a Senior Scientist at the International Nickel Company (1980–1984). Dr. Kang subsequently joined IBM at the Thomas J. Watson Research Center, where he has worked on microelectronic interconnection technologies and materials, and recently on conducting adhesives and Pb-free soldering technologies. He received an IBM Outstanding Quality Team Award in 1989, an IBM Research R&D Award in 1991, and an IBM Research External Honors Award in 1996. He is an author or coauthor of 34 U.S. patents and 105 technical papers. Dr. Kang is a Senior Member of the IEEE, and Chair of the Electronic Packaging and Interconnection Materials Committee of the Minerals, Metals, and Materials Society (TMS).

Paul A. Lauro IBM Research Division, Thomas J. Watson Research Center, P.O. Box 218, Yorktown Heights, New York 10598 (plauro@us.ibm.com). Mr. Lauro is a development engineer in the IBM Research Division. For the past 17 years, he has been a vital developer in the design and mechanical testing of integrated probe structures for chip testing and wafer-level burn-in. He is currently a member of a team working to characterize lead-free solders for microelectronics and chip packaging for electrical and thermal applications. Mr. Lauro is the author of more than fifty issued and pending patents covering various aspects of semiconductor packaging and testing. He served as an IBM Master Inventor for six years. Mr. Lauro's interests also include computer-aided design and micromechanical electronics.

**Da-Yuan Shih** *IBM Research Division, Thomas J. Watson Research Center, P.O. Box 218, Yorktown Heights, New York 10598 (dys@us.ibm.com)*. Dr. Shih is a Research Staff Member and Manager of the Electronic and Optical Packaging Department at the IBM Thomas J. Watson Research Center. He received a B.S. degree in physics from National Tsing-Hua University, Taiwan, and a Ph.D. degree in materials science from Syracuse University. Since joining IBM in 1981, Dr. Shih has worked on microelectronic packaging technologies, including structures, materials, processes, and, most recently, on lead-free solder technologies for packaging applications. He has received five IBM Research R&D Awards and three IBM Outstanding Technical Achievement Awards. Dr. Shih is an IBM Research Division Master Inventor.

Donald W. Henderson IBM Systems and Technology Group, 1701 North Street, Endicott, New York 13760 (donwhend@us.ibm.com). Dr. Henderson received his B.S. degree in electrical engineering from the Moore School at the University of Pennsylvania in 1968. He received his M.S. degree in 1972 and his Ph.D. degree in 1980 from Cornell University in the field of materials science and engineering. After completing his graduate education, Dr. Henderson worked as an adjunct Assistant Professor and Senior Research Associate at Cornell University

for five years before joining IBM in 1985. Since that time, Dr. Henderson has worked in a variety of materials science areas related to physical metallurgy and mechanical properties of materials, as well as manufacturing process development. Most recently he has worked on the physical metallurgy and mechanical properties of Pb-free solder alloys and problems related to Pb-free electronic packaging development.

Karl J. Puttlitz 21 Central Avenue, Wappingers Falls, New York 12590 (KJPuttlitz@aol.com). Dr. Puttlitz recently retired from the IBM Corporate Staff, Somers, New York; he is now a lecturer and consultant. He received a Ph.D. degree from Michigan State University in metallurgy/materials science engineering in 1971. As the Corporate Lead (Pb) Reduction Program Manager, Dr. Puttlitz had global responsibility to ensure that all IBM products conformed to ROHS and similar environmental requirements. However, he spent the majority of his more than 43-year tenure at IBM in various microelectronic packaging development programs, particularly interconnection technology, including, from their inception, flip-chip solder joints. Dr Puttlitz coauthored and coedited two handbooks; he is credited with nearly 40 published inventions, including domestic and foreign patents, more than 25 technical journal articles and papers presented at international conferences, and numerous invited lectures/workshops given worldwide. He is a member of several technical societies and was elected a Fellow of both the Institute of Electrical and Electronics Engineers and the American Society of Materials International.